# Experiments on the structure and stability of mode-2 internal solitary-like waves propagating on an offset pycnocline

M. Carr, P. A. Davies, and R. P. Hoebers

Citation: Physics of Fluids (1994-present) **27**, 046602 (2015); doi: 10.1063/1.4916881
View online: http://dx.doi.org/10.1063/1.4916881
View Table of Contents: http://scitation.aip.org/content/aip/journal/pof2/27/4?ver=pdfcov
Published by the AIP Publishing



PHYSICS OF FLUIDS **27**, 046602 (2015)

# Experiments on the structure and stability of mode-2 internal solitary-like waves propagating on an offset pycnocline

M. Carr,[1,a)] P. A. Davies,[2] and R. P. Hoebers[3]
[1]*School of Mathematics and Statistics, University of St Andrews, St Andrews, KY16 9SS, United Kingdom*
[2]*Department of Civil Engineering, University of Dundee, Dundee, DD1 4HN, United Kingdom*
[3]*Department of Applied Physics, Eindhoven University of Technology, Eindhoven, The Netherlands*

(Received 7 October 2014; accepted 23 March 2015; published online 13 April 2015)

The structure and stability of mode-2 internal solitary-like waves is investigated experimentally. A rank-ordered train of mode-2 internal solitary waves is generated using a lock release configuration. The pycnocline is centred either on the mid-depth of the water column (the 0% offset case) or it is offset in the positive vertical direction by a fraction of 5%, 10%, or 20% of the total fluid depth. It is found that offsetting the pycnocline has little effect on the basic wave properties (e.g., wave speed, wave amplitude, and wavelength) but it does significantly affect wave stability. Instability takes the form of small K-H-like billows in the rear of the wave and small scale overturning in the core of the wave. In the 0% offset case, instability occurs on both the upper and lower interfaces of the pycnocline and is similar in extent and vigour over the two interfaces. As the offset percentage is increased, however, instability is more pronounced on the lower interface with little or no evidence of instability being observed on the upper interface. In the 20% offset case, a mode-1 tail is associated with the wave and the wave characteristics resemble qualitatively the recent field observations of Shroyer *et al.* ["Mode 2 waves on the continental shelf: Ephemeral components of the nonlinear internal wavefield," J. Geophys. Res. **115**, C07001, doi:10.1029/2009JC005605 (2010)]. © *2015 AIP Publishing LLC.* [http://dx.doi.org/10.1063/1.4916881]

## I. INTRODUCTION

Internal solitary waves (ISWs) are commonly observed in many of the world's stratified oceans.[1] The majority of observations are of the first baroclinic mode (mode-1) waves. ISWs of mode-1 displace isopycnals in one direction only and can either be waves of elevation or, more typically in the oceanic context, waves of depression. Mode-2 ISWs, on the other hand, displace isopycnals in opposite directions and are of two type: convex, in which case upper isopycnals are displaced upward and lower isopycnals are displaced downward or concave, where the opposite is true. Concave waves require a thick pycnocline and, as such, are seldom seen because of the rarity of such a configuration in the stratified oceans.[2] Convex mode-2 ISWs, also known as varicose, double-humped or bulge-shaped waves, on the other hand, have frequently been detected[3–12] and the number of recent observations suggests that they may be more prevalent than previously thought. Shroyer *et al.*[11] showed that, although mode-2 waves had less energy than mode-1 waves observed in the same region, the magnitudes of the wave-localized turbulent dissipation were similar in both cases. This suggests that mode-2 ISWs may have a significant effect on eroding the pycnocline and

a)Author to whom correspondence should be addressed. Electronic mail: magda.carr@st-and.ac.uk. Telephone: +44(1334)463715. Fax: +44(1334)463748.

 

hence on the vertical fluxes of heat and nutrients in the water column. Moreover, the amplitudes reported by Shroyer *et al.*[11] were large, ranging from 1.6 m to 7.5 m. Estimates of the corresponding non-dimensional amplitude, computed indirectly from echo sounder images presented in Shroyer *et al.*,[11] range from $2a/h_2 \approx 1.5 - 4$, where $a$ is taken to be the maximum displacement of an isopycnal and $h_2$ is the thickness of the pycnocline. Yang *et al.*[10] have observed mode-2 ISWs in the South China sea with amplitudes as large as 56 m (corresponding to an estimate of 1.45 for the non-dimensional amplitude—see Figure 2(a) of their paper). Such waves are thought to be able to transport mass over significant distances (see Brandt and Shipley[13] and references therein).

In addition to the field observations mentioned above, significant progress has been made in describing mode-2 ISWs through theoretical investigations,[14–17] numerical analyses,[18–22] and laboratory experiments.[13,15,16,23–26] So far as laboratory investigations are concerned, Davis and Acrivos[15] provide the first experimental study of mode-2 ISWs. They used a plunger to impulsively inject fluid into the pycnocline to generate a mode-2 wave and focussed on using experimentally determined propagation velocities and wave shapes to verify theoretical calculations. Kao and Pao[16] collapsed a mixed region of fluid into the pycnocline of a stratified fluid. The mixed fluid was located in the centre of the wave tank and was allowed to collapse to either side so that the interaction of the two oppositely propagating mode-2 ISWs could be investigated. Maxworthy[23] also generated mode-2 ISWs by the collapse method but he retained some form of stratification behind the lock release and carefully looked at the effect of the dimensions of the generating volume on the amplitude and number of waves generated. Stamp and Jacka[25] used a paddle to force mixed fluid through baffles into the pycnocline. They showed that small waves carried energy and momentum, whereas sufficiently large waves also carried mass. More recently, Mehta *et al.*[26] showed that mode-2 ISWs can be excited by, and in front of a gravity intrusion and Brandt and Shipley[13] used the lock release method to investigate mass transport by large amplitude mode-2 ISWs.

All previous laboratory studies and the majority of theoretical and numerical studies have concentrated on a stratification in which the centre of the pycnocline is located exactly at mid-depth in the water column. Yet this configuration is unlikely to occur in the field where most observations are for pycnoclines which are offset (from mid-depth) in the positive vertical direction. Moreover, field observations have shown that wave characteristics depend strongly on the strength and form of the stratification. In particular, Yang *et al.*[10] found that the occurrence and form of mode-2 ISWs varied with season and this was correlated with the seasonal change of local stratification.

Consideration of the effect upon mode-2 waves of an offset of the pycnocline from the mid-depth of the fluid appears in the recent numerical work of Olsthoorn *et al.*[27] who investigated the consequences of offset for the structural characteristics of the wave. They found that the essential aspects of the wave generation process remained unchanged but noted that the waves, once formed, could be accompanied by a mode 1 tail and were asymmetric in form. They concluded that the cores of mode-2 ISWs are different from their mode-1 counterparts and argued that an accurate characterization on both laboratory and field scales should account for core asymmetry across the pycnocline centre. The present work is inspired by their paper and offers insight into core asymmetry in mode-2 ISWs on the laboratory scale. In addition, the waves that are described herein are shown to have remarkable similarities with the recent field observations of Shroyer *et al.*[11] The waves are generated using a lock release configuration and cases are considered in which the pycnocline in the main section of the tank has both a zero and non-zero offset. This is the first experimental study in which non-zero offsets have been considered.

The paper is organized as follows. In Sec. II, the experimental arrangement and measurement techniques are described. In Sec. III A, the experimental observations are presented and in Sec. III B, the effect of offsetting the pycnocline is discussed. In Sec. III C, quantitative results are presented and finally in Sec. IV, a summary and discussion are given.

## II. THE EXPERIMENTAL STUDY

### A. Experimental arrangement

Figure 1 shows a sketch of the experimental arrangement; a tank 6.4 m long ($L$), 0.4 m wide ($W$), 0.6 m high, and of rectangular cross section was divided into two sections by a vertical gate

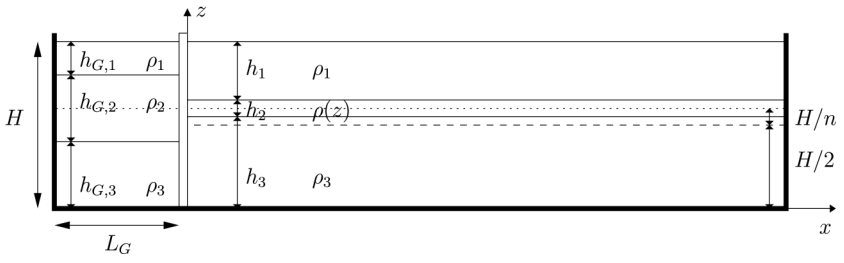


FIG. 1. Schematic diagram of experimental arrangement.

situated a distance $L_G$ from one end and extending to the bottom of the tank to isolate a fixed volume $WL_GH$ of fluid from the main chamber (where $H$ is the total fluid depth). Within a Cartesian coordinate system $(x, y, z)$, the $x$ and $z$ directions denote, respectively, the horizontal direction of wave propagation and the vertical direction anti-parallel to the gravitational acceleration vector $\mathbf{g} = (0, 0, -g)$. The origin is chosen such that $x = 0$ coincides with the horizontal location of the gate and $z = 0$ coincides with the lower solid boundary of the water column. The background stratification in the main part of the tank consisted of upper and lower layers of miscible homogeneous fluid of densities $\rho_1$ and $\rho_3$, respectively, and undisturbed thicknesses $h_1$ and $h_3$, respectively. The pycnocline had an undisturbed thickness of $h_2$ and the density, $\rho(z)$, varied as a linear function of $z$. The lower layer was filled first with a prepared solution of brine of prescribed density $\rho_3$ (typically 1048 kg m$^{-3}$). The top two layers were then carefully added via a floating sponge arrangement by directly filling with brine of density $\rho_1$ (typically 1025 kg m$^{-3}$).

Behind the gate were layers of density $\rho_{1,2,3}$ and thicknesses $h_{G,1}$, $h_{G,2}$, and $h_{G,3}$, respectively, and $\rho_2 = (\rho_1 + \rho_3)/2$ was set to be the mean density. The elevation of the central level of the middle layers at both sides of the gate was aligned always to be coincident (see the dotted line in Figures 1 and 2). The total water depth was $H(= 0.4$ m) on both sides of the gate. Cases were run in which the mid-plane of the middle layer was located either at mid-depth $H/2$ (see dashed line in Figure 1), the so-called 0%-offset condition, or displaced upwards from the mid-depth by a fraction $H/n$ $(n = 5, 10, 20)$—henceforth delineated, respectively, as 20%, 10%, and 5% offset conditions. The profile of the stratification, on both sides of the gate, was measured via an array of high precision micro-conductivity probes.[28] Figures 3(a) and 3(b) provide examples in the 0% offset and 20% offset cases, respectively. The thickness of the pycnocline, $h_2$, and the vertical extent of the generating volume, $h_{G,2}$, were measured from the probe data as defined schematically in Figure 2.

The density difference, $\Delta\rho = \rho_3 - \rho_1$, between layers was kept approximately constant during the study, as was the total fluid depth $H$. Due to practical considerations, the densities $\rho_1$ and $\rho_3$

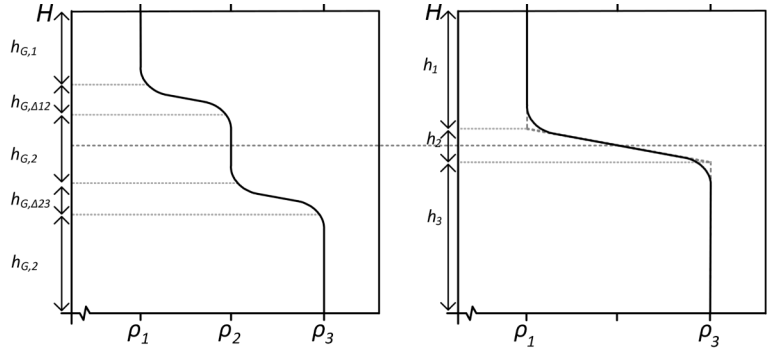


FIG. 2. Schematic diagram showing a typical stratification behind the gate (left hand plot) and in the main tank (right hand plot).

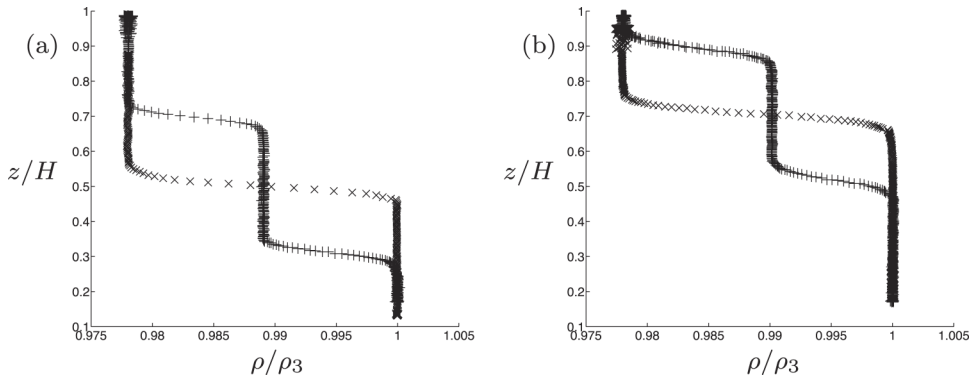


FIG. 3. An example of the stratification in the main section of the tank (×) and behind the gate (+) in (a) 0% offset case (260613) and (b) 20% offset case (030613).

varied slightly (<0.001%) from their prescribed values from run to run. Care was taken to make the thickness of the pycnocline, $h_2$, as small as possible. However, the precise formation of the pycnocline was difficult to control due to disturbances to the pycnocline during filling and differences in filling times. Parametric changes to the external conditions were introduced by changing (i) the pycnocline offset value, (ii) the thickness of the generating volume $h_{G,2}$, and (iii) the length of the generating volume $L_G$. Changes in the generating volume resulting from changes in either or both of $h_{G,2}$ and $L_G$ result primarily in changes in the prescribed amplitude of the ISW.

The experiment was initiated by the vertical removal of the gate which resulted in the generation of a train of mode-2 ISWs which propagated along the density interface into the main section of the tank. A Styrofoam lid was placed on top of the water column to aid comparison with numerical studies.[22,27] A total of 24 experiments was performed of which 19 are presented here. Table I provides an overview of the parameter range investigated.

TABLE I. Experimental parameter range.

| Date | Offset (%) | $L_G$ (m) | $h_{G,2}$ (m) | $h_2$ (m) | $\Delta\rho$ (kg m$^{-3}$) | $c/c_0$ | $2a/h_2$ | No. of waves | Stable |
|---|---|---|---|---|---|---|---|---|---|
| 260413 | 0.0 | 0.74 | 0.039 | 0.032 | 23 | 1.49 | 1.29 | 4-5 | Yes |
| 070513 | −0.4 | 0.74 | 0.064 | 0.030 | 23 | 1.86 | 2.20 | 2-3 | Marginal |
| 080613 | 0.7 | 0.30 | 0.066 | 0.032 | 23 | 1.67 | 1.66 | 2-3 | Yes |
| 220513 | −0.4 | 0.30 | 0.097 | 0.037 | 23 | 1.82 | 1.67 | 2-3 | Yes |
| 040713 | −0.1 | 0.30 | 0.095 | 0.030 | 22 | 1.83 | 2.03 | 2-3 | Marginal |
| 260613 | 0.5 | 0.30 | 0.129 | 0.030 | 23 | 1.83 | 2.36 | 2-3 | No |
| 280313 | 0.8 | 0.74 | 0.104 | 0.021 | 23 | 2.41 | 4.15 | 1-2 | No |
| 120613 | 4.9 | 0.30 | 0.066 | 0.033 | 23 | 1.55 | 1.61 | 2-3 | Yes |
| 240513 | 4.0 | 0.30 | 0.099 | 0.038 | 23 | 1.71 | 1.77 | 2-3 | Marginal |
| 070613 | 5.2 | 0.30 | 0.127 | 0.031 | 23 | 1.81 | 2.26 | 2-3 | No |
| 190613 | 10.3 | 0.30 | 0.063 | 0.028 | 23 | 1.62 | 1.66 | 2-3 | Yes |
| 280513 | 10.2 | 0.30 | 0.091 | 0.033 | 24 | 1.68 | 1.90 | 2-3 | Marginal |
| 210613 | 9.6 | 0.30 | 0.125 | 0.027 | 23 | 1.91 | 2.59 | 2 | No |
| 180613 | 19.1 | 0.30 | 0.062 | 0.031 | 23 | 1.58 | 1.46 | 3 | Yes |
| 250613 | 20.2 | 0.30 | 0.068 | 0.032 | 23 | 1.50 | 1.42 | 3 | Yes |
| 160513 | 20.5 | 0.30 | 0.075 | 0.042 | 23 | 1.42 | 1.55 | 2-3 | No |
| 030613 | 20.7 | 0.30 | 0.117 | 0.033 | 23 | 1.84 | 2.25 | 1-2 | No |
| 030513 | 19.2 | 0.74 | 0.067 | 0.029 | 23 | 1.78 | 2.18 | 2-3 | No |
| 180413 | 19.5 | 0.74 | 0.116 | 0.028 | 22 | 2.05 | 3.27 | 1-2 | No |

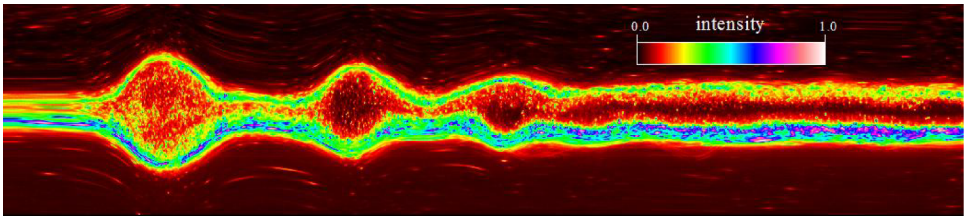


FIG. 4. Time series of light intensity from experiment 070513 taken at $x = 3.965$ m. The vertical extent is $z \in [0.121, 0.287]$ m and the horizontal extent is $\Delta t = 34.7$ s.

### B. Measurement technique

Particle image velocimetry (PIV) was used to visualize and quantify the synoptic velocity field $(u, w)$ in a given two-dimensional $(x, z)$ slice of the flow. To implement PIV, a vertical section in the mid-plane of the tank was illuminated by a continuous, collimated light sheet from an array of light boxes placed below the (transparent) base of the tank. The light sheet had a thickness of approximately 10 mm. Motions within this vertical light sheet were viewed and recorded from the side using 3 fixed digital video cameras set up outside the tank, each had a spatial resolution of $1372 \times 1372$ pixels. The water column in the main tank only was seeded with light-reflecting tracer particles of "Pliolite" having diameters in the range 150–300 $\mu$m. The particles had a buoyancy range such that they were neutrally buoyant throughout the depth of the water column. The 3 cameras were positioned to overlap with one another and to be level with the pycnocline to avoid distortion and perspective errors in this portion of the flow field.

The resulting video records of the flow field were processed using the software package *DigiFlow*.[29] The development of the interface was monitored using the time series function of *DigiFlow*, by tracking the changes with time of the pixel values in a given column of digitized images extracted from the camera record, for example, see Figure 4. The images were analysed using *DigiFlow* and estimates of the amplitude and the time at which the interface reached maximum displacement were then derived. The amplitude of the leading wave at its peak and trough were taken, respectively, to be the maximum displacement of the upper and lower isopycnals of the pycnocline, see Figure 5. This process was repeated at three fixed locations $x_{1,2,3}$ on any given camera over evenly spaced horizontal distances, enabling an average value for the upper amplitude, $a_u$, and lower amplitude, $a_l$, to be calculated. The variance in measuring the amplitude was 7%.

A distance versus time plot was generated using $x_{1,2,3}$ over all three cameras to get estimates of the wave celerity, $c_u$ and $c_l$, based on the measurements at the wave peak and the wave trough, respectively. The variance in measuring wave speed in this way was less than 1%. The upper and lower wavelengths, $\lambda_u$ and $\lambda_l$, respectively, were defined as the half-width at the height where the upper and lower amplitudes were half their maximum values. The measurements were restricted to the front half of the wave to avoid difficulties and ambiguities associated with asymmetry and/or the existence of a mode-1 tail in the rear part of the wave. The variance in measuring the wavelength was 7%.

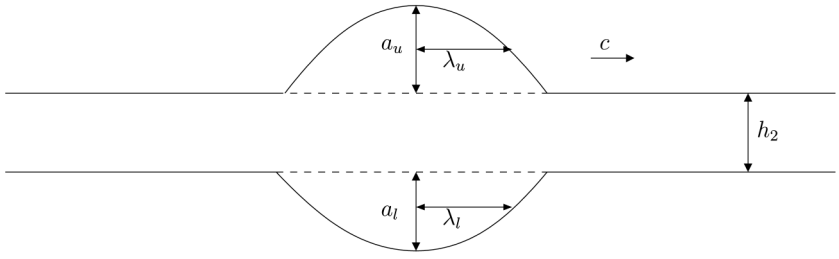


FIG. 5. Schematic diagram of the leading mode-2 wave detailing its characteristic variables.

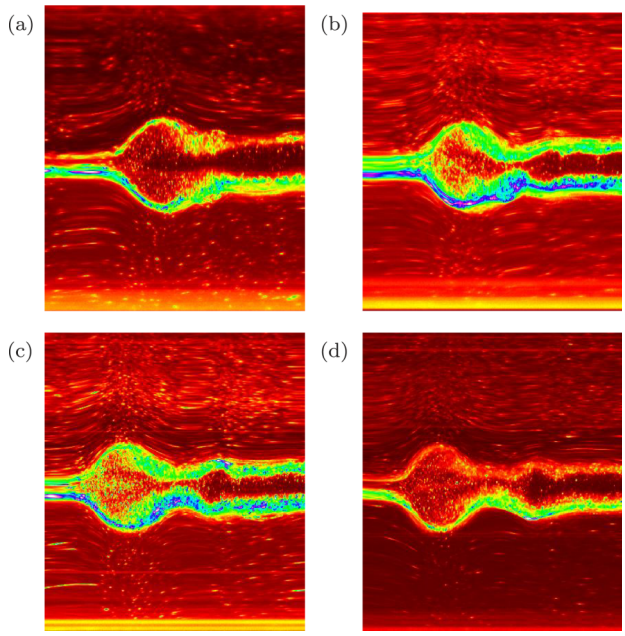


FIG. 6. Time series from experiment 280313. Each panel has a vertical extent of $z \in [0.023, 0.386]$ m ($z/H \in [0.06, 0.97]$) and a horizontal extent of $\Delta t = 15.8$ s and were taken at (a) $x = 3.16$ m ($x/H = 7.90$), (b) $x = 4.15$ m ($x/H = 10.38$), (c) $x = 4.44$ m ($x/H = 11.10$), and (d) $x = 4.73$ m ($x/H = 11.83$).

## III. EXPERIMENTAL RESULTS

### A. Experimental observations

A train of mode-2 ISWs was generated which propagated along the channel. The waves were rank-ordered in amplitude and, in some cases, the leading (large) wave was unstable. The instability

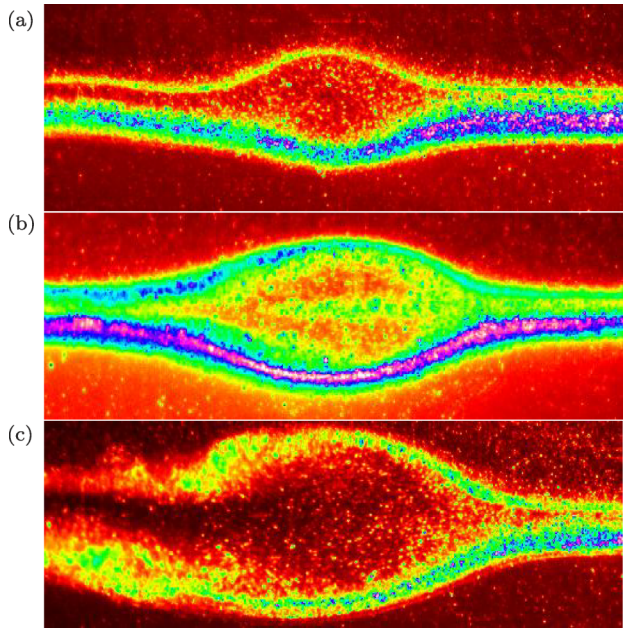


FIG. 7. Still images taken from experiments (a) 260413 ($2a/h_2 = 1.29$), (b) 040713 ($2a/h_2 = 2.03$), and (c) 280313 ($2a/h_2 = 4.15$). Each field of view has a vertical extent of $z \in [0.14, 0.26]$ m ($z/H \in [0.35, 0.65]$) and a horizontal extent of $x \in [3.68, 4.06]$ m ($x/H \in [9.20, 10.15]$).

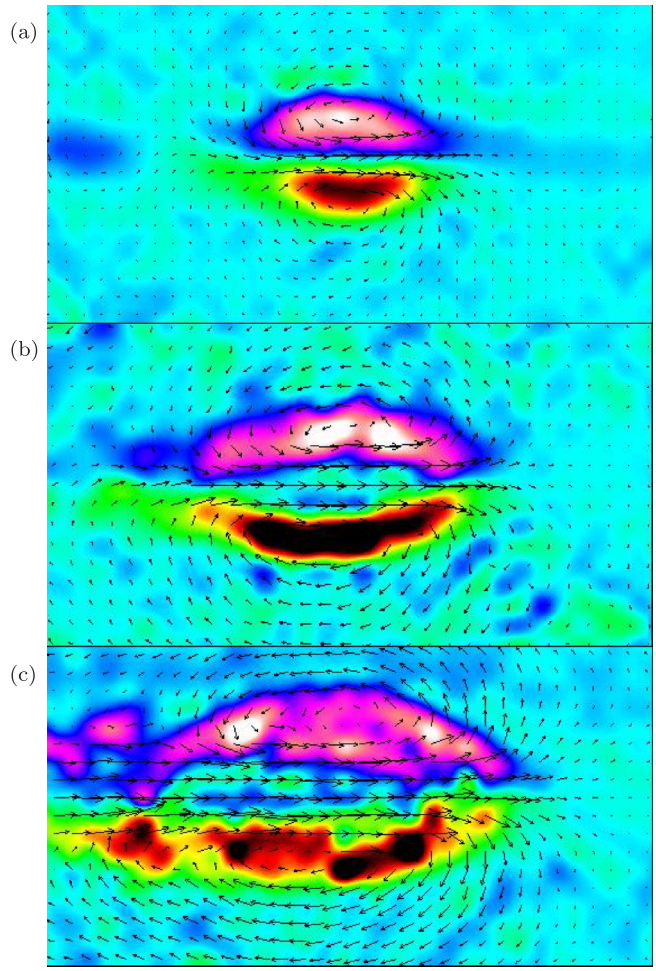


FIG. 8. Velocity (vector) and vorticity (background color map) fields corresponding to the waves shown in Figure 7. Each field of view has a vertical extent of $z \in [0.1, 0.3]$ m ($z/H \in [0.25, 0.75]$) and a horizontal extent of $x \in [3.68, 4.06]$ m ($x/H \in [9.20, 10.15]$). The color scheme is the same as that employed in Figure 4 with black and white corresponding to vorticity values of $-2.5$ s$^{-1}$ and 2.5 s$^{-1}$, respectively.

took the form of small scale overturning within the core of the wave along with shear instabilities (K-H like) in the rear of the leading wave. Prior to a given run, the main section of the wave tank was seeded with neutrally buoyant light reflecting tracer particles while the fluid behind the gate was never seeded (although it did contain some seeding when water was recycled from previous experiments). In all observations, particles were seen within the recirculating regions of the wave train while the tail of the wave was clear, suggesting that fluid was entrained into the wave core as the wave propagated while the tail was essentially (unseeded) fluid from behind the gate, see Figure 4 for illustration. Figure 4 is a time series of light intensity, showing the typical form of a stable wave (070513). Light intensity in Figure 4 is displayed by a false color scheme on a scale of zero to one as indicated by the color bar. In this and subsequent time series images (Figures 6, 11, and 16), the wave can be thought of as propagating from right to left. In all other figures, the waves are presented in the laboratory frame and propagate from left to right. In observations of flows exhibiting instability, fluid was observed to be not only entrained into the core but also subsequently mixed and ejected from the rear of the recirculating region. These observations are in excellent agreement with the previous laboratory investigations of Maxworthy[23,30] and Stamp and Jacka,[25] and the numerical observations of Salloum *et al.*[22]

To be in keeping with the literature,[22,23,25] characteristic length, density, and velocity scales are taken, respectively, to be the pycnocline half-thickness, $h_2/2$, the density difference, $\Delta\rho$, and the

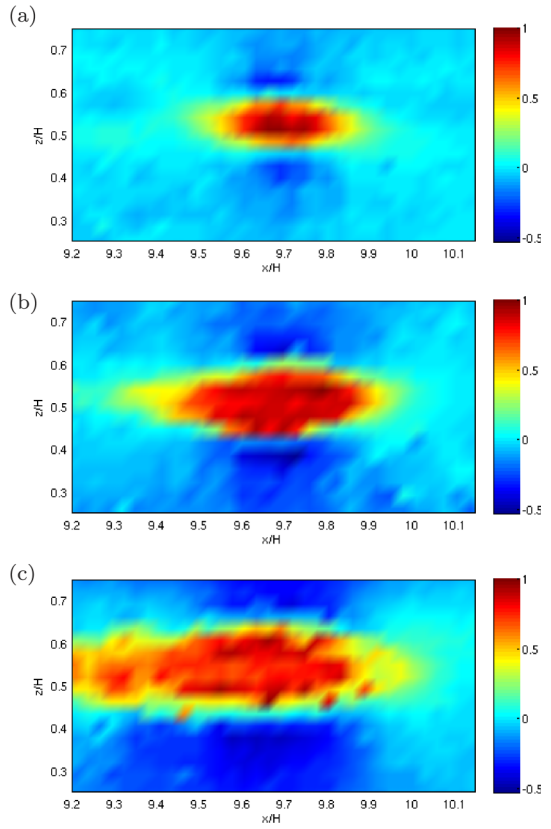


FIG. 9. Horizontal velocity field non-dimensionalised by measured wave speed $c$, for the waves shown in Figures 7 and 8.

celerity $c_0$ of a long infinitesimal mode-2 wave, viz,

$$c_0 = \frac{1}{2}\left(\frac{g h_2 \Delta\rho}{2\rho_2}\right)^{1/2},$$

where $g$ is the acceleration due to gravity. The corresponding Reynolds number, $Re \equiv c_0 h_2/2\nu$, where $\nu$ is the kinematic viscosity of water, was in the range 242 – 710. Over a range of $Re \in [25, 400]$, Salloum *et al.*[22] found that variation in the Reynolds number had little effect on the basic wave properties and, moreover, any trends essentially saturated at $Re = 400$. Hence, at least for the range of parameters of the laboratory cases presented here, variation in the Reynolds number is not expected to greatly influence the flow dynamics. Unless stated otherwise, all measures refer to those of the leading wave.

Table I lists the experimental runs and states how many waves were observed on a given train and whether the leading wave was stable. The data suggest that increasing the vertical extent, $h_{G,2}$, of the generating volume results in a larger amplitude leading wave with fewer waves in the tail (cf. 260413 070513, cf. 250613 160513 030613, and cf. 030513 180413). Moreover, increasing the horizontal extent, $L_G$, of the generating volume results in a larger amplitude leading wave with the number of waves in the tail remaining the same for the range investigated (cf. 070513 080613, cf. 030513 250613, and cf. 180413 030613). These findings are contrary to Maxworthy[23] who found that the number of waves produced increased as both the vertical and horizontal extent of the generating volume were increased. In the unstable experiments reported in this study, the number of waves on a given train could change over the observation time. Typically, instability decayed with evolution and in the process, a mode-2 wave could form in the wake of the leading wave. Figure 6 is included to illustrate such fission. In Figure 6, four time series are presented from an unstable, 0% offset experiment (280313). The four different time series were generated at horizontal locations of (a) $x = 3.16$ m ($x/H = 7.90$), (b) $x = 4.15$ m ($x/H = 10.38$), (c) $x = 4.44$ m ($x/H = 11.10$), and

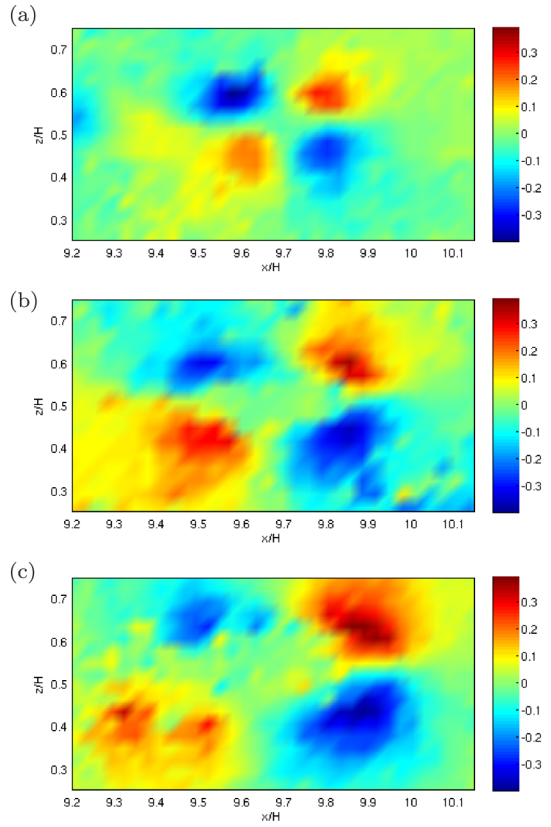


FIG. 10. Vertical velocity field non-dimensionalised by measured wave speed $c$, for the waves shown in Figures 7 and 8.

(d) $x = 4.73$ m ($x/H = 11.83$). Initially, there is only one mode-2 wave and it is unstable in the rear (see Figure 6(a) and the extended version in Figure 16(a)). As the wave propagates along the tank, the billowing associated with the instability decays and a second mode-2 wave is generated in the wake of the leading wave (Figures 6(b) and 6(c)). The second wave is smaller in amplitude than the leading wave, and as a result, as the wave train propagates further down the tank, the distance between the two mode-2 waves increases (Figure 6(d)). This fission effect may be one cause for the discrepancy in findings with Maxworthy.[23] Doing an exact comparison with Maxworthy[23] and classifying the number of waves that were generated for a given starting condition was not the aim of this study; hence, it is difficult to attribute the exact cause of the contrary findings.

Brandt and Shipley[13] classified the waves they saw into three types, namely, small amplitude ($1 < 2a/h_2 \leq 2$) with a smooth front face; large amplitude ($2 < 2a/h_2 < 4$) with an open

TABLE II. Comparison with the numerical results of Olsthoorn *et al.*[27]

| Expt. | Offset (%) | $L_G$ (m) | $h_{G,2}$ (m) | $l_1$ (m) | $l_2$ (m) | $l_3$ (m) | $a_1$ (m) | $a_2$ (m) | $a_3$ (m) |
|---|---|---|---|---|---|---|---|---|---|
| Numerical | 0.0 | 0.35 | 0.128 | 5.4 | 4.42 | 3.75 | 0.035 | 0.021 | 0.011 |
| 040713 | −0.1 | 0.30 | 0.095 | 5.4 | 4.60 | 4.11 | 0.033 | 0.014 | 0.099 |
| 260613 | 0.5 | 0.30 | 0.129 | 5.4 | 4.72 | … | 0.035 | 0.022 | … |
| Numerical | 5.0 | 0.35 | 0.128 | 5.4 | 4.42 | 3.75 | 0.035 | … | … |
| 240513 | 4.0 | 0.30 | 0.099 | 5.4 | 4.52 | … | 0.036 | … | … |
| 070613 | 5.2 | 0.30 | 0.127 | 5.4 | 4.72 | 4.24 | 0.035 | … | … |
| Numerical | 20.0 | 0.35 | 0.128 | 5.1 | 4.33 | … | 0.035 | … | … |
| 030613 | 20.7 | 0.30 | 0.117 | 5.1 | 4.34 | … | 0.035 | … | … |

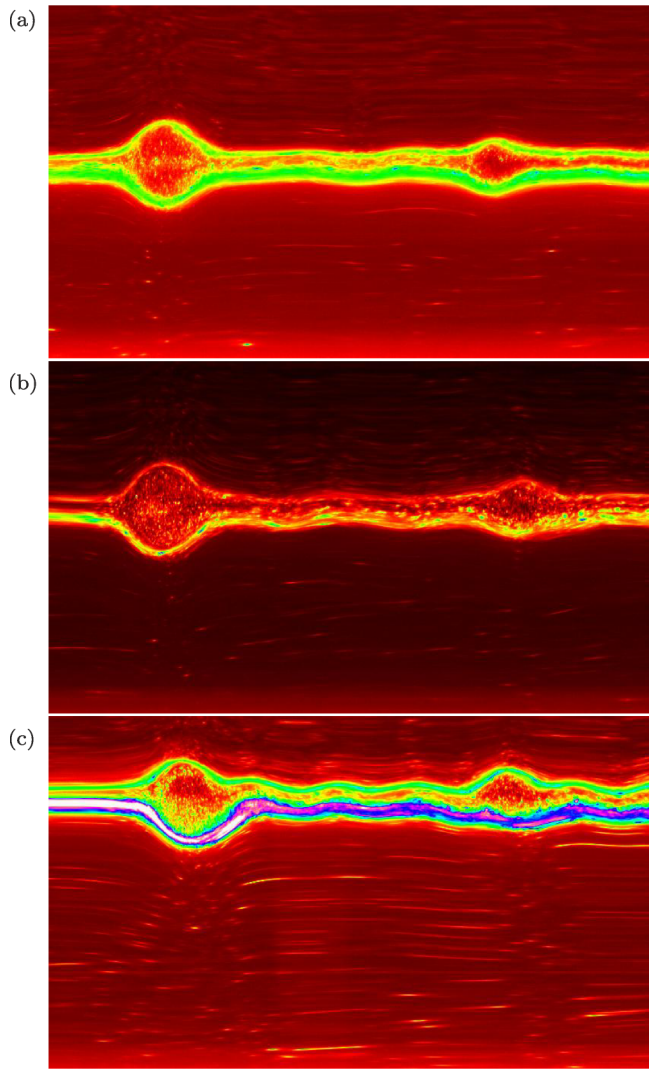


FIG. 11. Time series from experiments (a) 040713 (0% offset), (b) 240513 (5% offset), and (c) 160513 (20% offset). Each panel has a vertical extent of $z \in [0.03, 0.37]$ m ($z/H \in [0.08, 0.93]$), a horizontal extent of $\Delta t = 26.333$ s, and were taken at $x = 4.3$ m ($x/H = 10.75$).

mouth, leading edge "PacMan" opening where external fluid was entrained, dividing the core; and very-large amplitude ($2a/h_2 \geq 4$), with a smooth front face and an unstable rear. The present observations showed excellent agreement with Brandt and Shipley[13] and are illustrated in Figure 7. Figure 7 shows still images from experiments with a 0% offset and non-dimensional amplitudes of (a) $2a/h_2 = 1.29$, (b) $2a/h_2 = 2.03$, and (c) $2a/h_2 = 4.15$. The three different waves show the same characteristics as described in Brandt and Shipley[13] for their respective amplitudes.

Brandt and Shipley[13] did not report the wave characteristic as being transient but rather being clearly one of the three types over the period in which they observed them. This was not the case here and analysing streaklines confirmed that often waves which appeared to be "PacMan"-like at the first camera were "smooth" faced by the time they appeared at the third camera. For flows such as these that are unsteady, however, it is known that caution should be exercised (e.g., Tritton[31]) in interpreting comparisons between dye observations (which Brandt and Shipley[13] performed) and particle tracks and streaklines. Note that in Figure 7(a), there is a weak mode-1 tail associated with the mode-2 wave despite this experiment being classified as a 0% offset case and it being known[25,27] that such stratifications (with perfect vertical symmetry) cannot support mode-1 waves.

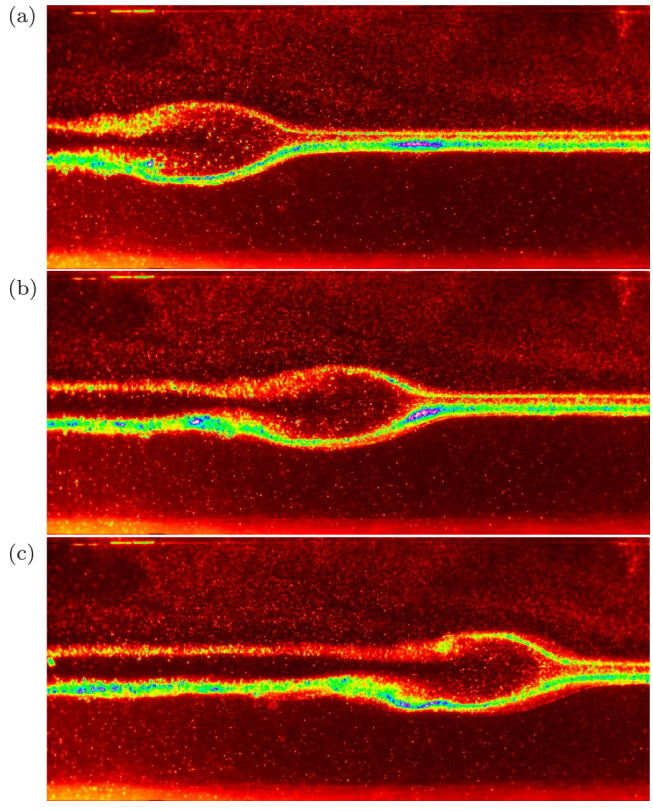


FIG. 12. A sequence of still images from experiment 280313 (0% offset condition). Each field of view has a vertical extent of $z \in [0.023, 0.386]$ m ($z/H \in [0.06, 0.97]$) and a horizontal extent of $x \in [3.075, 3.907]$ m ($x/H \in [7.69, 9.77]$). The time interval between images is $\Delta t = 3.333$ s.

In the laboratory, however, it was not possible to produce a perfectly symmetric stratification, due primarily to the experimental error associated with measuring the stratification and a minor slope on the channel geometry.

Brandt and Shipley[13] concentrated on dye experiments in order to obtain measurements of mass transport while here the emphasis was on seeding the flow so that the velocity field could be ascertained via PIV. In Figure 8, the velocity and vorticity fields are shown for the three waves depicted in Figure 7. The background color map represents vorticity while the velocity field is illustrated by vectors. Note that the vertical extent displayed is slightly larger than that given in Figure 7. In the largest amplitude case (Figure 8(c)), the K-H like instability in the rear of the wave can be seen as a secondary vortex behind the main circulating cell.

In Figures 9 and 10, the horizontal and vertical velocity components, non-dimensionalised by the measured wave speed $c$, are displayed, respectively, for the waves depicted in Figure 8. The horizontal velocity field has a core like structure in all three amplitude cases. In the small amplitude case, $2a/h_2 = 1.29$ (Figure 9(a)), the horizontal velocity reaches a maximum in the centre of the core. However, in the larger amplitude cases, $2a/h_2 = 2.03$ (Figure 9(b)) and $2a/h_2 = 4.15$ (Figure 9(c)), this is not the case and the velocity maximum is not concentrated in the centre of the core. In the large amplitude case ($2a/h_2 = 2.03$), the difference is attributed to the "tongue" of fluid in the "PacMan" example (Figure 7(b)) which entrains external fluid and divides the core. In the very large amplitude case ($2a/h_2 = 4.15$), it is attributed to the fact that this wave was unstable and fluid within the core is being mixed. In Figure 9, it can also be seen that the maximum value of $u/c$ is close to and sometimes exceeds a value of 1. It was found that in all the waves investigated, there were instances in which the maximum value of $u/c$ exceeded 1. It is well known that for mode-1 ISWs with $u/c > 1$, the waves develop trapped cores and can be subject to convective instability.[32,33]

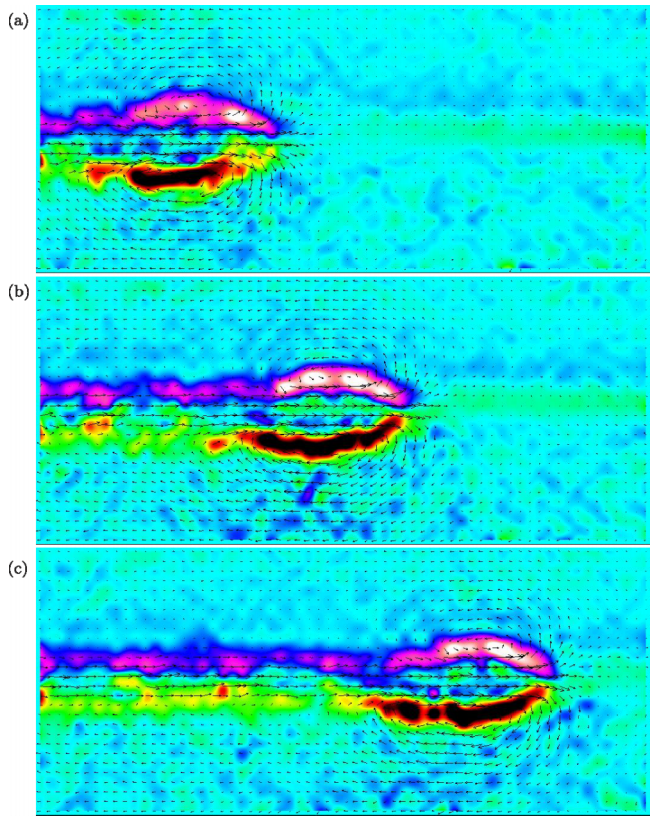


FIG. 13. Velocity (vector) and vorticity (background color map) fields corresponding to the wave shown in Figure 12. The color scheme is the same as that employed in Figure 4 with black and white corresponding to vorticity values of $-2.5\ s^{-1}$ and $2.5\ s^{-1}$, respectively.

### B. Effect of offsetting the pycnocline

Table II provides a comparison of the measured characteristic dimensions (see below) of the mode-2 wave trains with the predictions of the numerical simulations of Olsthoorn *et al.*[27] Olsthoorn *et al.*[27] performed a numerical investigation of the effect of offsetting the pycnocline centre on the structural characteristics of mode-2 ISWs. Note that in their work, Olsthoorn *et al.*[27] offset the pycnocline in the negative $z$ direction. The positive-negative offset cases are equivalent under the Boussinesq approximation provided that the distance of the pycnocline centre from mid-depth is the same in the two cases. Estimates of the horizontal and vertical extent of the generating volume in the numerical work are taken from Figure 3 in Olsthoorn *et al.*[27] The location of the leading and subsequent waves on a train is denoted by $l_1, l_2$, and $l_3$, respectively, while their corresponding amplitudes are denoted by $a_1, a_2$, and $a_3$, respectively, and are taken to be the maximum displacement of a displayed isopycnal in Figures 4 and 6 of Olsthoorn *et al.*[27] To make a comparison, the time at which the leading wave in an experiment was located at $l_1$ was noted and from the time code, the location of $l_2$ and $l_3$ could be determined from subsequent cameras. As previously noted, the waves were often asymmetric, so in all cases the location of the wave peak (as opposed to the wave trough) was used to determine the horizontal locations. Excellent agreement is seen between the wave amplitudes but there is some discrepancy on the spacing between waves on a given train. The laboratory waves were consistently closer together on a given train than the numerical counterparts. These differences are not surprising as the initial conditions were not exactly matched, see the variance in $L_G$ and $h_{G,2}$, and the generation technique was different in the two studies. In the laboratory, a solid gate was removed to initiate the experiment, whereas in the numerical work, the mixed fluid was simply allowed to collapse. Despite such differences, the agreement between the observations and the numerical work is remarkably good.

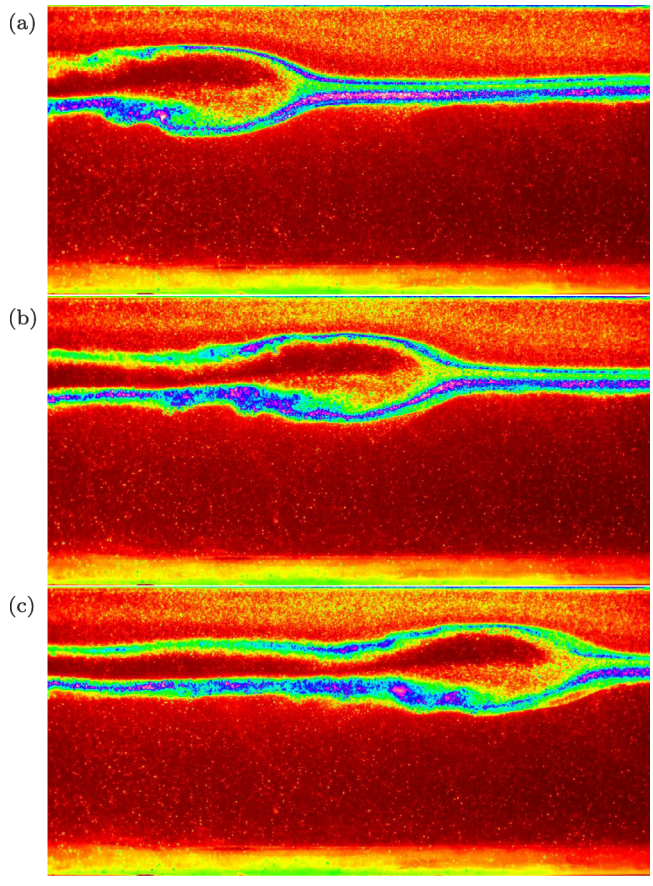


FIG. 14. A sequence of still images from experiment 180413 (20% offset condition). Each field of view has a vertical extent of $z \in [0.023, 0.386]$ m ($z/H \in [0.06, 0.97]$) and a horizontal extent of $x \in [3.075, 3.907]$ m ($x/H \in [7.69, 9.77]$). The time interval between images is $\Delta t = 3.333$ s.

To assess the effect of offsetting the pycnocline on wave stability, experiments 040713 (0% offset), 240513 (5% offset), and 160513 (20% offset) can be compared in Table I and Figure 11. Comparison in Table I implies that the occurrence and the strength of the motion resulting from instability increase with the offset percentage. In the 0% offset case (Figure 11(a)), the wave was stable, symmetric, and had no mode 1 tail associated with it. In the 5% offset case (Figure 11(b)), the wave was marginally unstable (cannot be seen from figure), it had slight asymmetry and it had a small mode 1 tail associated with it. However, in the 20% offset case (Figure 11(c)) the wave was unstable (cannot be seen from figure), clearly asymmetric, and it had a mode 1 tail associated with it. The instability was fairly weak and took the form of K-H like billows in the rear of the wave on the lower pycnocline interface only. The occurrence of asymmetry and a mode 1 tail in the 20% offset case are in excellent agreement with the findings of Olsthoorn *et al.*,[27] for example, see their Figures 6 and 9. Note in Figure 6 of Olsthoorn *et al.*[27] that instability is displayed in the 5% offset case but not in the 20% offset case. The reason for this is simply to do with the levels of isopycnals that were displayed in their Figure 6 (personal communication with Olsthoorn). Figure 11 of their paper confirms that they too saw evidence of instability in the 20% offset cases.

To discuss instability in more detail and the effect of offsetting, in particular, on its occurrence and manifestation, Figures 12–15 are presented. Figures 12 and 14 show a sequence of still images from two different experiments showing instability and in which all parameters were held approximately constant except for the offset percentage (cf. 280313 and 180413 in Table I). Figures 13 and 15 show the corresponding velocity and vorticity fields for Figures 12 and 14, respectively. In the 0% offset case (Figures 12 and 13), evidence of instability was seen on both the top and bottom of the pycnocline

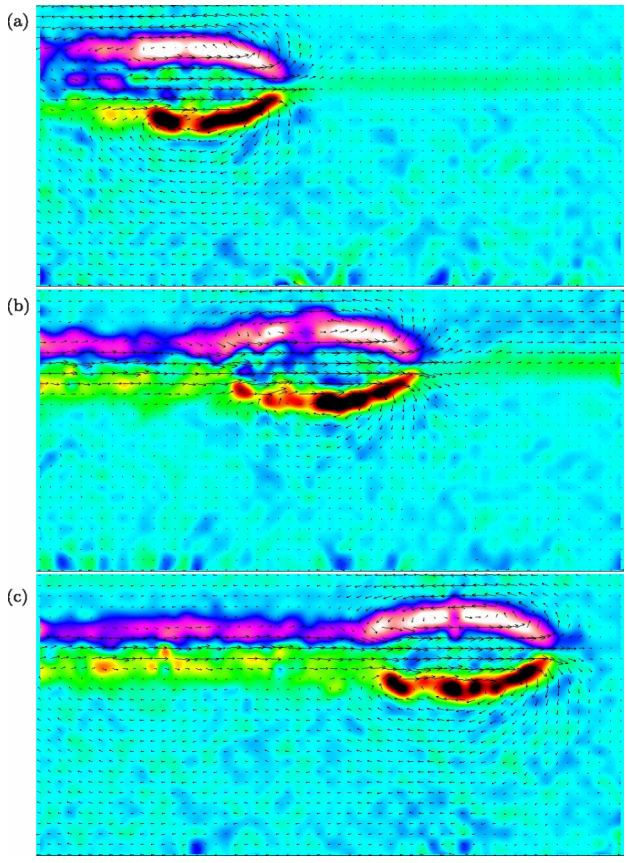


FIG. 15. Velocity (vector) and vorticity (background color map) fields corresponding to the wave shown in Figure 14. The color scheme is the same as that employed in Figure 4 with black and white corresponding to vorticity values of $-2.5\ s^{-1}$ and $2.5\ s^{-1}$, respectively.

in the rear of the wave (in these images, the wave propagates from left to right). The form and vigour of the instability-induced overturning motions changed with time but, typically, the properties of these motions were comparable on the upper and lower surfaces. In the 20% offset case (Figures 14 and 15), evidence of instability was also on both interfaces but, in this instance, the associated flow features were relatively stronger in intensity on the lower boundary. A discussion of this observation is delayed until Sec. IV. The vigour of the instability-induced flow in the 20% offset case was greater than in the 0% case. This trend (increasing offset percentage resulting in increased occurrence of instability and increased associated overturning in the flow) was seen throughout the experiments.

Figure 16 shows two time series for the two experiments shown in Figures 12 and 14. In the 0% offset case (Figure 16(a)), the wave shape and the form of the flow structures associated with instability in the tail look fairly symmetric. The core of the wave is evenly seeded in the upper and lower sections (implying even entrainment over the vertical extent of the core) and the tail is flat (as expected). In contrast, in the 20% offset case (Figure 16(b)), the wave and the instability are clearly asymmetric, there is more seeding in the lower half of the core (implying that entrainment is more pronounced there) and there is a mode-1 tail associated with the wave. These characteristics (in the 20% case) are very similar to field observations.[3,11,17] More discussion of this is given in Sec. IV.

### C. Quantitative results

Figure 17 is a stability diagram showing how offset percentage and wave amplitude are related to wave stability. Wave observations are classified as stable (+), unstable (o), or marginally unstable (∗). A wave was classified as marginally unstable if the instability was weak and/or transient during an experiment. It can be seen that (a) the critical amplitude required for instability is a function

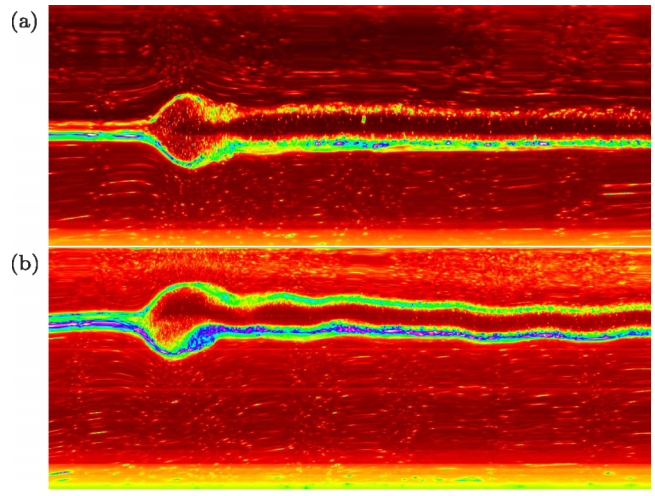


FIG. 16. Time series from experiment (a) 280313 (0% offset) and (b) 180413 (20% offset). Each panel has a vertical extent of $z \in [0.023, 0.386]$ m ($z/H \in [0.06, 0.97]$) and a horizontal extent of $\Delta t = 37.1$ s, and were taken at $x = 3.16$ m ($x/H = 7.90$) and $x = 3.18$ m ($x/H = 7.95$), respectively.

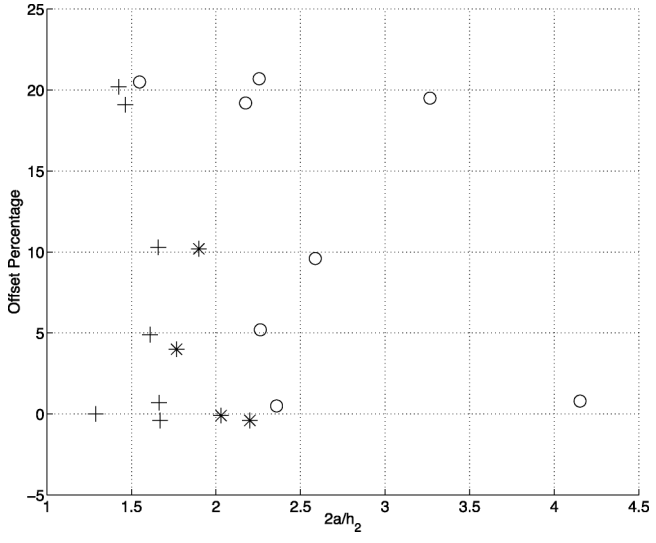


FIG. 17. Offset percentage versus wave amplitude. Stable (+), marginally unstable (∗), and unstable (o) observations are plotted.

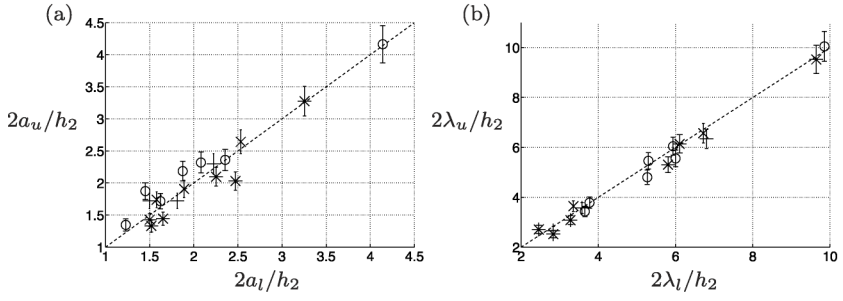


FIG. 18. Measurements of (a) the upper and lower values of the amplitude and (b) the upper and lower values of the wavelength in the 0% (∘), 5% (+), 10% (×), and 20% (∗) offset cases. The dashed line in (a) denotes $a_u = a_l$ and in (b) denotes $\lambda_u = \lambda_l$.

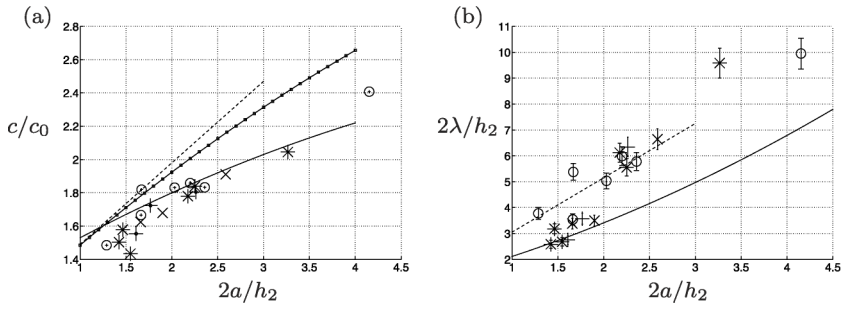


FIG. 19. (a) Wave speed and (b) wavelength versus wave amplitude in the 0% (∘), 5% (+), 10% (×), and 20% (∗) offset cases. The dashed line denotes the linear fit from Stamp and Jacka,[25] the square line is the quadratic fit from Maxworthy,[30] and the dotted line the quadratic fit from Brandt and Shipley.[13]

of the offset percentage and (b) the higher the degree of offset, the lower the critical amplitude. In the 0% offset cases, the critical amplitude was found to be 2.36. This is in excellent agreement with Maxworthy,[30] see his Figure 5(b), which displays a value of approximately 2.2. It is also in good agreement with Salloum *et al.*[22] who report a value of 2.75 for the flow within the wave to drop below the minimum gradient Richardson number instability criterion ($Ri_g = 1/4$), where $Ri_g$ is defined in the usual way as $Ri_g = N^2(z)/(du/dz)^2$. Here, $N(z)$ represents the vertical ($z$) variation in the buoyancy frequency $N$ and $du/dz$ is the vertical shear in the horizontal velocity.

Figure 18 shows plots of (a) the non-dimensional upper amplitude, $2a_u/h_2$, versus the non-dimensional lower amplitude, $2a_l/h_2$ and (b) the non-dimensional upper wavelength, $2\lambda_u/h_2$, versus the non-dimensional lower wavelength, $2\lambda_l/h_2$, for varying offset values. Error bars are added to the data points to show the variance in the respective measures. Figure 18(a) suggests that the upper amplitude is consistently larger than the lower amplitude measure in the 0% offset case (∘) and vice versa in the 20% offset case (∗). Within the bounds of error, these findings are in agreement with Stamp and Jacka[25] in the 0% offset case (see their Figure 6(a)) and Olsthoorn *et al.*[27] in the 20% offset case (see their Figure 6(c)). Figure 18(b) suggests that, for all cases, there is no significant difference between the upper and lower wavelength values. In the 0% offset cases, this is in agreement with Stamp and Jacka[25] (see their Figure 6(b)).

Figure 19 shows plots of (a) the non-dimensional wave speed, $c/c_0$ and (b) the non-dimensional wavelength, $2\lambda/h_2$, versus the non-dimensional amplitude, $2a/h_2$, for varying offset values, where $c = (c_u + c_l)/2$, $\lambda = (\lambda_u + \lambda_l)/2$, and $a = (a_u + a_l)/2$ are defined to be the average wave speed, average wavelength, and average wave amplitude, respectively, of the leading mode-2 bulge (wave). The dashed line denotes the linear fit from Stamp and Jacka,[25] while the square and dotted lines are quadratic fits from Maxworthy[30] and Brandt and Shipley,[13] respectively. Note that error bars have not been added to the data set in Figure 19(a) as they were smaller than the marker size. Given the

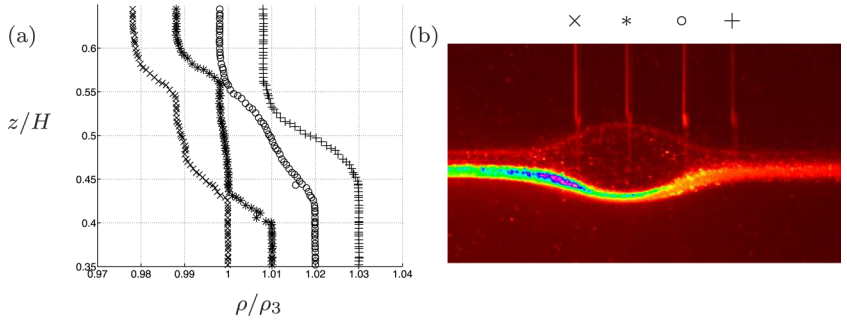


FIG. 20. (a) Density profile through the core of a stable wave (080613) and (b) the location of the 4 probes used to measure the strike. For illustration purposes, the profiles in (a) have been staggered by adding a constant value of $\rho/\rho_3 = 0.01, 0.02$, and 0.03 for probes (∗), (∘), and (+), respectively.

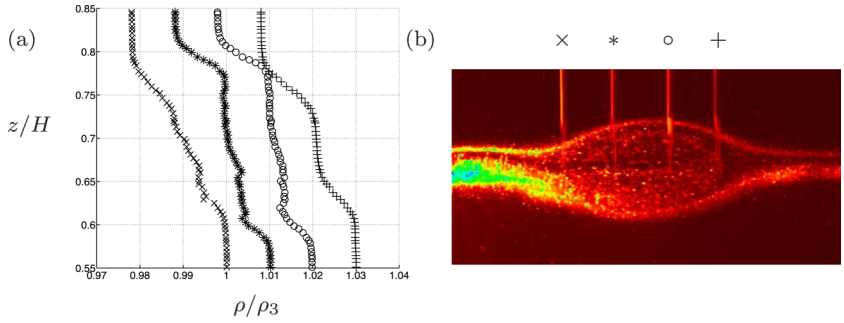


FIG. 21. (a) Density profile through the core of an unstable wave (030613) and (b) the location of the 4 probes used to measure the strike. For illustration purposes, the profiles in (a) have been staggered by adding a constant value of $\rho/\rho_3 = 0.01, 0.02$, and $0.03$ for probes $(*)$, $(\circ)$, and $(+)$, respectively.

good agreement between data sets, it can be concluded that introducing an offset has little influence on the relationship between wave speed, wavelength, and wave amplitude. These findings are in good agreement with Olsthoorn *et al.*[27] who found that the essential aspects of the wave generation process remained unchanged when offsetting the pycnocline.

Figure 20 shows (a) density profiles within the core of a stable wave (080613) and (b) the location of the four probes used to measure the profiles within the wave. For illustration purposes, the profiles have been staggered by adding a constant value of $\rho/\rho_3 = 0.01,\ 0.02$, and $0.03$ for probes $(*)$, $(\circ)$, and $(+)$, respectively. The wave is travelling from right to left. The data from probes $(+)$ and $(\circ)$ show that ahead of the wave and just into the front of the wave, the pycnocline is simply stretched by the presence of the wave. Probe $(*)$ shows that in the centre of the wave, there is a region within the core of the wave in which the fluid is well mixed. Similarly, probe $(\times)$ shows that towards the rear there is a well mixed region within the core.

Figure 21 shows counterpart data to those shown in Fig. 20, but for an unstable wave (030613). Probes $(\circ)$ and $(*)$ show evidence of small scale overturning (denser fluid can be seen over lighter fluid) toward the bottom of both profiles. The degree of overturning can be assessed by considering the related Thorpe scale.[34] To do this, the unstable profiles are reordered into stable (monotonic) ones using a bubble sort routine.[35] Each data point $\rho_n$ initially at a depth $z_n$ is assigned a new depth $z_m$ in the reordered profile. The Thorpe displacement is defined to be the difference $d'_n = z_m - z_n$ and the Thorpe scale $L_t$ is defined as the root mean square of this quantity.[34] In Table III, a comparison of the Thorpe scale in two different experiments in which everything is held approximately fixed except the offset percentage is given. The vertical extent over which a given profile was reordered is denoted by $L_z$ and $L_{tmax}$ is the maximum Thorpe displacement $d'$ in a given profile. Note that the Thorpe scale, $L_t$, is two orders of magnitude less than the vertical extent over which it is measured, implying that the related overturning is relatively weak. The two data sets are chosen for comparison as the second and third probes struck the waves at similar relative positions, namely, just ahead and just behind the wave peak, respectively. However, the data cannot be compared exactly between runs as the horizontal position at which the probes strike the wave are somewhat arbitrary and as such, analysis of these data must be taken in context. Table III suggests that as the offset percentage increases so does the non-dimensional Thorpe scale $L_t/L_z$, a property that is in

TABLE III. Thorpe scale analysis.

| Expt. | Offset percentage | Probe | $L_z/a$ | $L_t/L_z$ | $L_t/L_{tmax}$ |
|---|---|---|---|---|---|
| 070613 | 5.2% | $\circ$ | 1.686 | 0.068 | 0.237 |
| 070613 | 5.2% | $*$ | 2.229 | 0.063 | 0.189 |
| 030613 | 20.7% | $\circ$ | 1.756 | 0.093 | 0.380 |
| 030613 | 20.7% | $*$ | 1.810 | 0.073 | 0.284 |

keeping with the argument above that the degree of instability (and hence overturning) increases with percentage offset.

## IV. SUMMARY AND DISCUSSION

An experimental study was undertaken in which a train of mode-2 internal solitary-like waves were generated using a lock release configuration. In the main section of the tank, the pycnocline was centred either on the mid-depth of the water column (the 0% offset case) or it was offset in the positive vertical direction by a fraction which corresponded to 5%, 10%, or 20% of the total water column depth. Behind the gate, the vertical and horizontal extent of the mixed layer used to generate the wave train was varied, and as a result, the amplitude and number of waves could be indirectly controlled. It was found that offsetting the pycnocline had little effect on the basic wave properties (e.g., wave speed, wave amplitude, and wavelength) but it did affect wave stability.

The critical amplitude required for instability was shown to decrease as the percentage offset increased (see Figure 17). In the 0% offset case, the critical amplitude was found to be 2.36, which is in very good agreement with the previous studies of Maxworthy[30] and Salloum *et al.*[22] who found values of 2.2 and 2.75, respectively. Instability took the form of small K-H like billows in the rear of the wave and weak overturning in the core of the wave. In the 0% offset case, instability occurred on both the upper and lower interfaces of the pycnocline. As the offset percentage was increased, however, the instability-induced overturning was more pronounced on the lower interface with little or no evidence of instability being observed on the upper interface (see Figures 14 and 16(b), for example). The reason for seeing such asymmetry is not clear. The data in Figure 18(a) suggest that the upper amplitude is smaller than the lower amplitude in the 20% offset cases ($*$). This effect was also seen in Olsthoorn *et al.*[27] (invert their Figure 6(c)). The presence of the solid upper boundary and the reduced upper layer thickness is expected to restrict the upper amplitude as the upper boundary is approached and this may provide an explanation as to why instability is less pronounced on the upper interface. An alternative explanation for the difference in instability conditions may be the skewness of the wave shape in the 20% offset cases (for example, see Figures 11(c) and 16(b)). Classifying the waves in terms of an asymmetry measure was investigated but it was not possible to ascertain a reliable measure with the given data.

Note that the numerical observation of instability in Olsthoorn *et al.*[27] also showed asymmetry. Instability only occurred on the interface which deviated into the thicker layer (in their case, the upper boundary as their waves were offset in the negative vertical direction) while the lower interface was not disturbed at all by instability. Moreover, the field observations of Shroyer *et al.*[11] (Figure 7(a)) and Farmer and Smith[3] (see Akylas and Grimshaw[17] Figure 2) also exhibit asymmetric instabilities. In particular, note that Figure 7(a) of Shroyer *et al.*[11] shows a mode-2 wave in the field with (i) a clear mode 1 tail associated with it and (ii) enhanced back scatter (instability) in the rear of the wave in the lower but not upper part of the wave. These characteristics are very similar to those observed in this laboratory study in the non-zero offset cases. It is well known, in the mode-1 case,[36,37] that instability depends on several factors. To fully understand the stability observations recorded here (and in the field), further theoretical and numerical investigation is needed.

It is also known from previous studies on mode-1 ISWs[32,38] that trapped cores only occur when significant stratification occurs near the surface/bed for ISWs of depression/elevation, and that if a region of mixed fluid is present at the boundary, trapped cores do not form. In analogy, more trapping is expected to occur in mode-2 ISWs if the pycnocline is continuously stratified, as opposed to being an intermediate density layer with two transition regions. This has implications for understanding mass transport in the ocean and warrants further investigation.

## ACKNOWLEDGMENTS

Technical support was provided at the University of Dundee by John Anderson. Much of the experimental work was undertaken as part of a short internship held by one of the authors (RH) with the support of a small maintenance grant from The University of Dundee. The authors would like to thank two anonymous referees for critical comments that have led to improvements in the paper.

[1] C. R. Jackson, *An Atlas of Internal Solitary-like Waves and their Properties*, 2nd ed. (Global Ocean Associates, 2004), see www.internalwaveatlas.com.
[2] Y. J. Yang, Y. C. Fang, T. Y. Tang, and S. R. Ramp, "Convex and concave types of second baroclinic mode internal solitary waves," Nonlinear Processes Geophys. **17**, 605 (2010).
[3] D. M. Farmer and J. D. Smith, "Tidal interaction of stratified flow with a sill in Knight Inlet," Deep-Sea Res., Part A **27A**, 239 (1980).
[4] K. V. Konyaev, K. D. Sabinin, and A. N. Serebryany, "Large-amplitude internal waves at the Mascarene Ridge in the Indian Ocean," Deep Sea Res., Part I **42**, 2075 (1995).
[5] T. F. Duda, J. F. Lynch, J. D. Irish, R. D. Beardsley, S. R. Ramp, C.-S. Chiu, T. Y. Tang, and Y. J. Yang, "Internal tide and nonlinear internal wave behaviour at the continental slope in the Northern South China Sea," IEEEE J. Oceanic Eng. **29**, 1105 (2004).
[6] Y. J. Yang, T. Y. Tang, M.-H. Chang, A. K. Liu, M.-K. Hsu, and S. R. Ramp, "Solitons northeast of Tung-Sha Island during the ASIAEX pilot studies," IEEEE J. Oceanic Eng. **29**, 1182 (2004).
[7] D. J. Bogucki, L. G. Redekopp, and J. Barth, "Internal solitary waves in the coastal mixing and optics 1996 experiement: Multimodal structure and resuspension," J. Geophys. Res. **110**, C02024, doi:10.1029/2003JC002253 (2005).
[8] K. Sabinin and A. Serebryany, "Intense short-period internal waves in the ocean," J. Mar. Res. **63**, 227 (2005).
[9] J. N. Moum, J. D. Nash, and J. M. Klymak, "Small-scale processes in the coastal ocean," Oceanography **21**, 22 (2008).
[10] Y. J. Yang, Y. C. Fang, M.-H. Chang, S. R. Ramp, C.-C. Kao, and T. Y. Tang, "Observations of second baroclinic mode internal solitary waves on the continental slope of the northern South China Sea," J. Geophys. Res. **114**, C10003, doi:10.1029/2009JC005318 (2009).
[11] E. L. Shroyer, J. N. Moum, and J. D. Nash, "Mode 2 waves on the continental shelf: Ephemeral components of the nonlinear internal wavefield," J. Geophys. Res. **115**, C07001, doi:10.1029/2009JC005605 (2010).
[12] S. R. Ramp, Y. J. Yang, D. B. Reeder, and F. L. Bahr, "Observations of a mode-2 nonlinear internal wave on the northern Heng-Chun Ridge south of Taiwan," J. Geophys. Res. **117**, C03043, doi:10.1029/2011JC007662 (2012).
[13] A. Brandt and K. R. Shipley, "Laboratory experiments on mass transport by large amplitude mode-2 internal solitary waves," Phys. Fluids. **26**, 046601 (2014).
[14] T. B. Benjamin, "Internal waves of permanent form in fluids of great depth," J. Fluid Mech. **29**, 559 (1967).
[15] R. E. Davis and A. Acrivos, "Solitary internal waves in deep water," J. Fluid Mech. **29**(3), 593 (1967).
[16] T. W. Kao and H.-P. Pao, "Wake collapse in the thermocline and internal solitary waves," J. Fluid Mech. **97**, 115 (1980).
[17] T. R. Akylas and R. H. J. Grimshaw, "Solitary internal waves with oscillatory tails," J. Fluid Mech. **242**, 279 (1992).
[18] K. K. Tung, T. F. Chan, and T. Kubota, "Large amplitude internal waves of permanent form," Stud. Appl. Math. **66**, 1 (1982).
[19] D. E. Terez and O. M. Knio, "Numerical simulations of large-amplitude internal solitary waves," J. Fluid Mech. **362**, 53 (1998).
[20] P.-O. Rusås and J. Grue, "Solitary waves and conjugate flows in a three-layer fluid," Eur. J. Mech., B: Fluids **21**, 185 (2002).
[21] M. Stastna and W. R. Peltier, "On the resonant generation of large-amplitude internal solitary and solitary-like waves," J. Fluid Mech. **543**, 267 (2005).
[22] M. Salloum, O. M. Knio, and A. Brandt, "Numerical simulation of mass transport in internal solitary waves," Phys. Fluids **24**, 016602 (2012).
[23] T. Maxworthy, "On the formation of nonlinear internal waves from the gravitaional collapse of mixed regions in two and three dimensions," J. Fluid Mech. **96**, 47 (1980).
[24] H. Honji, N. Matsunaga, Y. Sugihara, and K. Sakai, "Experimental observation of internal symmetric solitary waves in a two-layer fluid," Fluid Dyn. Res. **15**, 89 (1995).
[25] A. P. Stamp and M. Jacka, "Deep-water internal solitary waves," J. Fluid Mech. **305**, 347 (1995).
[26] A. P. Mehta, B. R. Sutherland, and P. J. Kyba, "Interfacial gravity currents. II. Wave excitation," Phys. Fluids **14**, 3558 (2002).
[27] J. Olsthoorn, A. Baglaenko, and M. Stastna, "Analysis of asymmetries in propagating mode-2 waves," Nonlinear Processes Geophys. **20**, 59 (2013).
[28] P. A. Davies, "Aspects of flow visualisation and density field monitoring of stratified flows," Opt. Lasers Eng. **16**, 311 (1992).
[29] S. B. Dalziel, M. Carr, J. K. Sveen, and P. A. Davies, "Simultaneous synthetic schlieren and PIV measurements for internal solitary waves," Meas. Sci. Technol. **18**, 533 (2007).
[30] T. Maxworthy, "Experiments on solitary internal Kelvin waves," J. Fluid Mech. **129**, 365 (1983).
[31] D. J. Tritton, *Physical Fluid Dynamics*, 2nd ed. (Oxford University Press, 1988).
[32] K. G. Lamb, "A numerical investigation of solitary internal waves with trapped cores formed via shoaling," J. Fluid Mech. **451**, 109 (2002).
[33] M. Carr, D. Fructus, J. Grue, A. Jensen, and P. A. Davies, "Convectively induced shear instability in large amplitude internal solitary waves," Phys. Fluids **20**, 126601 (2008).
[34] S. A. Thorpe, "Turbulence and mixing in a Scottish Loch," Philos. Trans. R. Soc. London, Ser. A **286**, 125 (1977).
[35] T. M. Dillon, "Vertical overturns: A comparison of Thorpe and Ozmidov length scales," J. Geophys. Res. **87**(C12), 9601, doi:10.1029/JC087iC12p09601 (1982).
[36] D. Fructus, M. Carr, J. Grue, A. Jensen, and P. A. Davies, "Shear-induced breaking of large internal solitary waves," J. Fluid Mech. **620**, 1 (2009).
[37] M. Carr, S. E. King, and D. G. Dritschel, "Numerical simulation of shear-induced instabilities in internal solitary waves," J. Fluid Mech. **683**, 263 (2011).
[38] K. G. Lamb, "Shoaling solitary internal waves: On a criterion for the formation of waves with trapped cores," J. Fluid Mech. **478**, 81 (2003).